*Journal of Sound and Vibration* (1996) **198**(2), 131–147

# THE REGULAR AND CHAOTIC MOTIONS OF A SYMMETRIC HEAVY GYROSCOPE WITH HARMONIC EXCITATION

Z.-M. Ge, H.-K. Chen and H.-H. Chen

*Institute of Mechanical Engineering, National Chaio Tung University, Hsinchu, Taiwan, Republic of China*

(*Received* 9 *June, and in final form* 14 *February* 1996)

The non-linear motion of a symmetric gyro mounted on a vibrating base is investigated, with particular emphasis on its long-term dynamic behaviour for a wide range of parameters. A single modal equation is used to analyze the qualitative behavior of the system. External disturbance appears as vertical harmonic motion of the support point and linear damping is assumed. The complete equation of motion is a non-linear non-autonomous one. The stability of the system has been studied by damped Mathieu equation theory and the Liapunov direct method. As the system is subjected to external disturbance, the Melnikov method is used to show the existence of chaotic motion. Finally, the bifurcation of the parameter dependent system is studied numerically. The time evolutions of the non-linear dynamical system responses are described in phase portraits via the Poincaré map technique. The occurrence and the nature of chaotic attractors are verified by evaluating Liapunov exponents and average power spectra. The effect of the gyroscope's spinning speed is also studied, and it is shown that the gyroscope's spin velocity $\omega_z$ has a significant effect on the dynamic behavior of the motion.



## 1. INTRODUCTION

Research in the area of gyro dynamics dates back about one hundred years, whereas the pioneering paper on the concept of chaotic motion in gyros was not presented until 1981 [1]. In this paper a detailed dynamic analysis was provided of a heavy symmetric gyro mounted on a vibrating base.

The concept of chaos was first introduced by Poincaré [2] to describe orbits in space mechanics. The chaotic behavior of fluids and gases was given by Lorenz [3]. Chaos occurs in mechanical or electrical oscillators, in rotating heated fluids, in chemical reactions and even in economic systems, etc. [4, 5]. Some modern techniques used in analyzing deterministic non-linear systems are numerical time solutions: Poincaré mapping, power spectrum analysis, the determination of the Liapunov exponents and an analytic method called the Melnikov method.

In this paper, a symmetric gyro mounted on a vibrating base is considered. A single modal equation of motion is used to analyze the dynamic behavior of the system. External disturbance appears as the vertical harmonic motion of the support point and linear damping is assumed. The complete equation of motion is a non-linear non-autonomous one. In this work, system stability is studied using the damped Mathieu equation theory [6] and the Liapunov direct method [7]. Since the system is subjected to external disturbance, the Melnikov method [8] is used to show the existence of chaotic motion. Finally, bifurcation of the parameter dependent system is studied numerically. The time



0022–460X/96/470131 + 17 $25.00/0 

via the Poincaré map technique. The occurrence and the nature of chaotic attractors are verified by evaluating Liapunov exponents and average power spectra. The effect of gyroscope's spin speed is also studied, and it is shown that the spin velocity $\omega_z$ of the the gyroscope has a significant effect on the dynamic behavior of the motion; e.g., a chaotic motion will become regular as the spin velocity of the gyroscope increases.

## 2. FORMULATION OF PROBLEM

The geometry of the problem under consideration is depicted in Figure 1. The motion of a symmetric gyro mounted on a vibrating base can be described by Euler's angles $\theta$, $\phi$ and $\psi$. By the Lagrangian approach, the Lagrangian has the expression

$$L = \tfrac{1}{2}I_1(\theta^2 + \phi^2 \sin^2\theta) + \tfrac{1}{2}I_3(\phi\cos\theta + \psi)^2 Mg(l + \bar{l}\sin\omega t)\cos\theta, \tag{1}$$

where $I_1$ and $I_3$ are the polar and equatorial moments of inertia of the symmetric gyroscope respectively, $Mg$ is the gravity force, $\bar{l}$ is the amplitude of the external excitation disturbance, and $\omega$ is the frequency of the external excitation disturbance. It is not difficult to see that the co-ordinates $\phi$ and $\psi$ are cyclic, as they are absent from the Lagrangian, which provides us with two first integrals of the motion expressing the conjugate momenta. The momentum integrals are

$$P_\phi = \frac{\partial L}{\partial\dot{\phi}} = I_1\dot{\phi}\sin^2\theta + I_3(\dot{\phi}\cos\theta + \dot{\psi})\cos\theta = \beta_\phi, \tag{2}$$

$$P_\psi = \frac{\partial L}{\partial\dot{\psi}} = I_3(\dot{\phi}\cos\theta + \dot{\psi}) = I_3\omega_z = \beta_\psi, \tag{3}$$

where $\omega_z$ is the gyroscope's spin velocity.

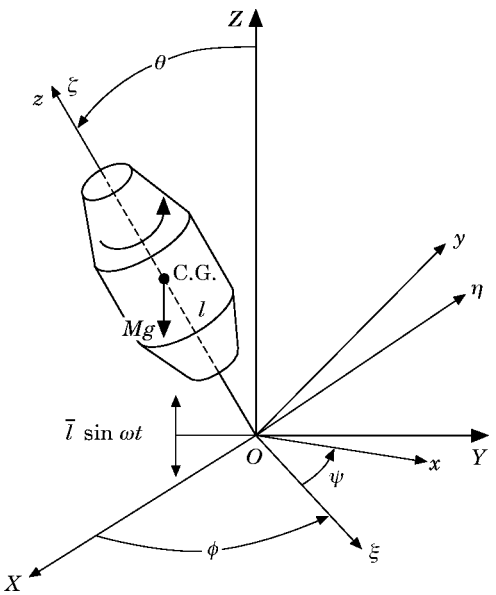


Figure 1. A schematic diagram of the physical system.

Now adopting Routh's procedure and using the above relation, the Routhian of the system becomes

$$R = L - \beta_\phi \dot{\phi} - \beta_\psi \dot{\psi} = \tfrac{1}{2} I_1 \dot{\theta}^2 - \left[ \frac{(\beta_\phi - \beta_\psi \cos\theta)^2}{2I_1 \sin^2\theta} + \frac{\beta_\phi^2}{2I_3} + Mg(l + \bar{l}\sin\omega t)\cos\theta \right], \quad (4)$$

which depends on the angle $\theta$ alone. For the trivial solution $\theta = 0$, which will be studied later, from equations (2) and (3), $\beta_\phi = \beta_\psi$ is automatically satisfied and is assumed to hold afterwards [9]. The dissipation function is also given by

$$F = \tfrac{1}{2} C \dot{\theta}^2. \quad (5)$$

The only equation of motion describing the system can be obtained from

$$\frac{\mathrm{d}}{\mathrm{d}t}\left(\frac{\partial R}{\partial \dot{\theta}}\right) - \frac{\partial R}{\partial \theta} + \frac{\partial F}{\partial \dot{\theta}} = 0, \quad (6)$$

allowing the system to be viewed as a single-degree-of-freedom system. The equation governing the gyroscope is given by

$$\ddot{\theta} + \frac{\beta_\phi^2}{I_1^2}\frac{(1-\cos\theta)^2}{\sin^3\theta} + \frac{C}{I_1}\dot{\theta} - \frac{Mgl}{I_1}\sin\theta = \frac{Mg\bar{l}}{I_1}\sin\omega t \sin\theta. \quad (7)$$

In convenient first order form, the normalized equations are

$$\dot{x}_1 = x_2, \qquad \dot{x}_2 = -\alpha^2 \frac{(1-\cos x_1)^2}{\sin^3 x_1} - cx_2 + \beta \sin x_1 + f \sin\omega t \sin x_1', \quad (8)$$

where

$$x_1 = \theta, \qquad x_2 = \dot{\theta}, \qquad \alpha = \beta_\phi / I_1 = I_3 \omega_z / I_1, \qquad c = C/I_1, \qquad \beta = Mgl/I_1, \qquad f = Mg\bar{l}/I_1. \quad (9)$$

## 3. STABILITY ANALYSIS

In this section, the local stability [10] and stability in a finite region of the solutions of the system are studied by the damped Mathieu equation theory and the Liapunov direct method respectively. A technique for determining local stability region for the damped Mathieu equation developed by Gunderson *et al*. [6] will be used to study stability. First, the solution $\theta = \dot{\theta} = 0$ is studied. If the nutation angle $\theta$ is sufficiently small, then $\sin\theta \approx \theta$ and $(1-\cos\theta)^2/\sin^3\theta \approx \theta/4$. Hence the equation of motion becomes

$$\ddot{\theta} + c\dot{\theta} + (\delta - f\sin\omega t)\theta = 0, \quad (10)$$

where $\delta = \alpha^2/4 - \beta$.

The problem is to find the relationships between $c$, $\delta$ and $f$ such that the solutions of this equation are asymptotically stable. However, if $2\tau = \omega t - \pi/2$, the equation becomes the damped Mathieu equation,

$$\frac{\mathrm{d}^2\theta}{\mathrm{d}\tau^2} + \frac{2c}{\omega}\frac{\mathrm{d}\theta}{\mathrm{d}\tau} + \left(\frac{4\delta}{\omega^2} - \frac{4f}{\omega^2}\cos 2\tau\right)\theta = 0. \quad (11)$$

According to the results by Gunderson *et al*. [6], if

$$f < c^2/2 + c\sqrt{\delta}, \quad (12)$$

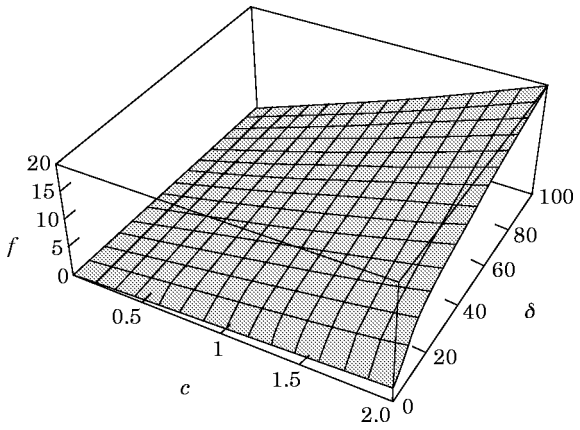


Figure 2. The damped Mathieu stable region.

is satisfied, the solutions are asymptotically locally stable. The stable region is the region below the surface shown in Figure 2.

Next, the stability of the system will be investigated by means of the Liapunov direct method briefly introduced here. This direct method requires constructing a function, $V(x)$, and its derivative such that they possess certain properties. When these properties of $V(x)$ and $\dot{V}(x)$ are demonstrated to exist, the stability behavior of motion is known. In general, the proper choice of $V(x)$ depends to an extent upon the experience, the ingenuity and often the good fortune of the analyst. The major task is to construct such a Liapunov function and to explain the physical meaning implicit in the sufficient conditions for stability obtained.

The equations of motion given above are deterministic, second order, non-linear and non-autonomous. It is a highly non-linear problem. For our purpose, the non-linear terms $(1 - \cos x_1)^2/\sin^3 x_1$ and $\sin x_1$ are expanded into power series of $x_1$:

$$\frac{(1 - \cos x_1)^2}{\sin^3 x_1} = \frac{x_1}{4} + \frac{x_1^3}{12} + O(x_1)^5, \qquad \sin x_1 = x_1 - \frac{x_1^3}{6} + O(x_1)^5. \tag{13, 14}$$

Hence the governing equations of the system are given by

$$\dot{x}_1 = x_2, \qquad \dot{x}_2 = -P(t)x_1 - cx_2 + Q(t)x_1^3 + O(x_1)^5, \tag{15}$$

where

$$P(t) = \frac{\alpha^2}{4} - \beta - f \sin \omega t, \qquad Q(t) = \frac{\alpha^2}{12} - \frac{\beta}{6} - \frac{f \sin \omega t}{6}. \tag{16}$$

Following the Liapunov stability analysis [7], first the fixed points of our system are examined. One finds that (A) $x_1 = x_2 = 0$ and (B) $x_1 = \pm\pi$, $x_2 = 0$ are fixed points for all parameter values.

For the fixed point (A), $(x_1, x_2) = (0, 0)$, this solution describes a motion in which one of the gyroscope's principal axes coincides with the local vertical axis. To study stability, let the disturbance of motion be

$$x_1 = \xi_1, \qquad x_2 = \xi_2. \tag{17}$$

Substituting (17) into (15), one obtains the equations of disturbance as follows:

$$\dot{\xi}_1 = \xi_2, \qquad \dot{\xi}_2 = -P(t)\xi_1 - c\xi_2 + Q(t)\xi_1^3 + O(\xi_i)^5. \tag{18}$$

In this case there is no physical intuition readily available to guide one in the choice of $V$. Thus (after possibly a great deal of trial and error), one might be led to try the Liapunov function candidate

$$V(t, \xi_1, \xi_2) = \tfrac{1}{2}P(t)\xi_1^2 + \tfrac{1}{2}\xi_2^2 + \xi_1\xi_2. \tag{19}$$

The Liapunov function $V$ is positive definite provided that

$$P(t) > 1; \tag{20}$$

i.e.,

$$\alpha^2/4 - \beta - f\sin\omega t > 1. \tag{21}$$

It is evident that the above inequality implies

$$\alpha^2/4 - \beta - 1 > f. \tag{22}$$

The total derivative of $-\dot{V}(x)$ is

$$-\dot{V}(t, \xi_1, \xi_2) = \left[P(t) - \frac{f\omega}{2}\cos\omega t\right]\xi_1^2 + c\xi_1\xi_2 + (c-1)\xi_2^2 + O(\xi_i)^3. \tag{23}$$

The requirements of $\dot{V}$ in the Liapunov direct method are

$$P(t) > \frac{f\omega}{2}\cos\omega t, \qquad c > 1, \qquad 4(c-1)\left(P(t) - \frac{f\omega}{2}\cos\omega t\right) > c^2, \tag{24}$$

i.e.,

$$c > 1, \qquad \frac{\alpha^2}{4} - \beta - \frac{c^2}{4(c-1)} > f\sqrt{1 + \frac{\omega^2}{4}}\,. \tag{25}$$

According to the Liapunov stability theorem [7] and the new theorem proposed by Cveticanin [11], inequalities (25) are sufficient conditions for system stability, and $(x_1, x_2) = (0, 0)$ is asymptotically stable equilibrium.

For the fixed points (B), $(x_1, x_2) = (\pm\pi, 0)$, which represents what is an inverted gyro's motion. To study the stability, let the distributed motion be

$$x_1 = \pm\pi + \xi_1, \qquad x_2 = \xi_2. \tag{26}$$

Substituting (26) into (15), one finds that

$$\dot{\xi}_1 = \xi_2, \qquad \dot{\xi}_2 = -(P - 3\pi^2 Q)\xi_1 - c\xi_2 \pm 3\pi Q\xi_1^2 + Q\xi_1^3 + O(\xi_i)^3. \tag{27}$$

Similarly, the Liapunov function $V$ is taken as

$$V(t, \xi_1, \xi_2) = \tfrac{1}{2}(P - 3\pi^2 Q)\xi_1^2 + \tfrac{1}{2}\xi_2^2 + \xi_1\xi_2. \tag{28}$$

The total derivative of $-V$ is

$$-\mathrm{d}V/\mathrm{d}t = [P - 3\pi^2 Q + \tfrac{1}{2}(\pi^2/2 - 1)f\omega \cos \omega t]\xi_1^2 + (c-1)\xi_2^2 + c\xi_1\xi_2 + O(\xi_i)^3. \quad (29)$$

The requirements for both $V$ and $-V$ are positive definite:

$$c > 1, \qquad \frac{\alpha^2}{4}(1-\pi^2) + \left(\frac{\pi^2}{2} - 1\right)\beta > \left\{\frac{c^2}{4(c-1)} + f\sqrt{\left(\frac{\pi^2}{2} - 1\right)^2\left(1 + \frac{\omega^2}{4}\right)}\right\}. \quad (30)$$

By the Liapunov theorem, inequalities (30) are the sufficient conditions for system stability, and the fixed point $(x_1, x_2) = (\pm\pi, 0)$, which are asymptotically stable equilibriums.

It is evident that stability has been established. In general, for a given system parameters $\beta$ and $c$ are fixed, whereas the normalized amplitude $f$ and the frequency $\omega$ of the external harmonic excitation and the spin velocity $\omega_z[\alpha = (I_3/I_1)\omega_z]$ vary. An inspection of inequalities (25) indicates that stability can be achieved simply by increasing the spin velocity when the gyroscope is spinning in an upright position. Similarily, inequality (30) points out that stability can be achieved as the spin velocity is slow for an inverted gyro.

## 4. DETECTING CHAOTIC DYNAMICS BY MELNIKOV METHOD

Previous studies have established the stability of a symmetric gyro mounted on a vibrating base. These investigations induced interest in the question of whether the critical system parameter values at which regular periodic motion changes into chaotic motion can be estimated theoretically by simple closed form critera, not involving numerical integration. To simplify the question, assume that $\beta$ is equal to one, and that $\alpha^2 \approx 0$, the spin velocity of the gyro being sufficiently small; the dissipation $c = \epsilon\bar{c}$ is also assumed to be small. Hence, system (7) can be expressed in the form

$$\dot{x}_1 = x_2, \qquad \dot{x}_2 = -\epsilon\bar{c}x_2 + (1 + F(t)) \sin x_1. \quad (31)$$

The behavior of the above system for two cases of the specific form of $F(t)$ will be examined.

(a) $F(t) = \epsilon\bar{f} \sin \omega t$, where $\omega$, $\bar{f} > 0$. This means that the disturbance amplitude is assumed to be small. The perturbation form yields

$$\dot{x}_1 = x_2, \qquad \dot{x}_2 = \sin x_1 + \epsilon(\bar{f} \sin \omega t \sin x_1 - \bar{c}x_2). \quad (32)$$

For $\epsilon = 0$, the system can be reduced to a Hamiltonian system. The stable and unstable manifold structure of the Hamiltonian system can be obtained using the Poincaré map method. One notes that the homoclinic orbits divide stable regions from the unstable ones.

For $\epsilon \neq 0$ the invariant manifolds split, and transverse intersections can occur. In the case of no transverse intersections the stable manifolds define a stable region with a smooth boundary. When intersections of stable and unstable manifolds occur, they give rise to infinitely many so-called homoclinic intersection points. In such a case one can show that in the Poincaré section the stable and unstable manifolds are stretched and folded into a horseshoe shape. The Melnikov function is used to measure the distance between stable and unstable manifolds when the distance is small [8]. The central idea of the Melnikov function is to find the Melnikov function $M(t_0)$. If this function vanishes for certain parameter values, then intersections between stable and unstable manifolds are near the

saddle points. For $\epsilon \neq 0$, equations (31) can be viewed as a Hamiltonian system with a perturbation

$$\dot{x} = f_0(x) + \epsilon g_0(x, t), \tag{33}$$

where

$$x = (x_1, x_2), \qquad f_0(x) = (x_2, \sin x_1), \qquad g_0(x) = (0, \bar{f} \sin \omega t \sin x_1 - \bar{c} x_2). \tag{34}$$

For $\epsilon = 0$, the system has centers at $(x_1, x_2) = (\pm\pi, 0)$ and a saddle point at $(0, 0)$ (see Appendix A). The Hamiltonian of the system is

$$H = \tfrac{1}{2} x_2^2 - \cos(x_1 + \pi). \tag{35}$$

Hence the unperturbed homoclinic orbits are given by

$$q_+^0(t) = (2 \tan^{-1}(\sinh t) - \pi), 2 \operatorname{sech} t), \qquad q_+^0(t) = -q_-^0(t). \tag{36}$$

By computing the Melnikov function of $q_+^0(t)$ (the computation for $q_-^0$ is identical), the Melnikov function is given by

$$\begin{aligned} M(t_0) &= \int_{-\infty}^{\infty} x_2(t - t_0)\{\bar{f} \sin \omega t \sin [2 \tan^{-1}(\sinh (t - t_0) - \pi] - \bar{c} x_2(t - t_0)\} \, \mathrm{d}t \\ &= -4\bar{f} \int_{-\infty}^{\infty} \sin \omega t \operatorname{sech}^2 (t - t_0) \tanh (t - t_0) \, \mathrm{d}t - 4\bar{c} \int_{-\infty}^{\infty} \operatorname{sech}^2 (t - t_0) \, \mathrm{d}t \\ &= -4\bar{f} M_a - 4\bar{c} M_b, \end{aligned} \tag{37}$$

where

$$M_a = \int_{-\infty}^{\infty} \sin \omega t \operatorname{sech}^2 (t - t_0) \tanh (t - t_0) \, \mathrm{d}t, \qquad M_b = \int_{-\infty}^{\infty} \operatorname{sech}^2 (t - t_0) \, \mathrm{d}t. \tag{38}$$

For convenience of computation, $M_a$ can be rearranged as

$$\begin{aligned} M_a &= \int_{-\infty}^{\infty} \sin \omega(t - t_0)(\operatorname{sech}^2 t) \tanh t \, \mathrm{d}t \\ &= \int_{-\infty}^{\infty} [\sin \omega t \cos \omega t_0 - \cos \omega t \sin \omega t_0](\operatorname{sech}^2 t) \tanh t \, \mathrm{d}t. \end{aligned} \tag{39}$$

Since the odd part of an integrand integrates to zero, $M_a$ can be written simply as

$$M_a = \left\{ \int_{-\infty}^{\infty} [\sin \omega t (\operatorname{sech}^2 t) \tanh t] \mathrm{d}t \right\} \cos \omega t_0. \tag{40}$$

The integrals $M_a$ and $M_b$ can be evaluated by the residue method to yield

$$M_a = -\bar{f} \omega^2 \operatorname{cosech} (\pi\omega/2) \cos \omega t_0, \qquad M_b = 2. \tag{41}$$

Then, the final form for $M(t_0)$ is

$$M(t_0) = 2\pi \bar{f} \omega^2 \operatorname{cosech}(\pi\omega/2) \cos \omega t_0 - 8\bar{c}. \tag{42}$$

The terms $2\pi\bar{f}\omega^2$ cosech $(\pi\omega/2)$ and $8\bar{c}$ are constant, as the parameter values $(\bar{f}, \bar{c}, \omega)$ are fixed. Hence, as $t_0$ is varied, $M(t_0)$ oscillates at about a mean value of $-8\bar{c}$ in an harmonic manner and with an amplitude of $2\pi\bar{f}\omega^2$ cosech $(\pi\omega/2)$. It is quite simple to determine the behavior of stable and unstable manifolds. The two perturbed manifolds will touch transversely when $M(t_0)$ has a simple zero, and the critical value of the amplitude $\bar{f}$ is given by

$$\bar{f} = \left| \frac{4\bar{c}}{\pi\omega^2 \text{ cosech } (\pi\omega/2)} \right|. \tag{43}$$

This yields

$$\bar{f}/\bar{c} = R(\omega), \tag{44}$$

with

$$R(\omega) = \frac{4}{\pi\omega^2} \sinh\left(\frac{\pi\omega}{2}\right). \tag{45}$$

The above relationship characterizes the onset of homoclinic bifurcation with an accuracy $O(1)$ for sufficiently small $\epsilon$. For $\bar{f}/\bar{c} > R(\omega)$, there exist transverse homoclinic intersection points between the stable and unstable manifolds of the saddle point (0, 0) for the Poincaré map of equations (32), which means the occurrence of chaos. Regions of chaos from theory and numerical simulation are shown in Figure 3. It is evident that good agreement between theory and numerical simulation has been demonstrated.

(b) $F(t) = \gamma \sin \epsilon\omega t$, where $\gamma, \omega > 0$. That means that there is no restriction on the amplitude of the excitation, but the frequency of excitation must be $O(\epsilon)$. From equations (31) the system can be written as

$$\dot{x}_1 = x_2, \qquad \dot{x}_2 = (1 + \gamma \sin Z) \sin x_1 - \epsilon\bar{c}x_2, \qquad \dot{Z} = \epsilon\omega. \tag{46}$$

Clearly, the above system cannot be analyzed by the traditional Melnikov method. A technique similar to Melnikov's for detecting the presence of orbits homoclinic to hyperbolic periodic orbits and normally hyperbolic invariant tori in a class of ordinary differential equations was developed by Wiggins [12]. A brief explanation is now given. Consider the system

$$\begin{aligned} \dot{x}_1 &= f_1(x_1, x_2, z) + \epsilon g_1(x_1, x_2, z, t; \mu), \\ \dot{x}_2 &= f_2(x_1, x_2, z) + \epsilon g_2(x_1, x_2, z, t; \mu), \\ \dot{z} &= \epsilon\omega, \end{aligned} \tag{47}$$

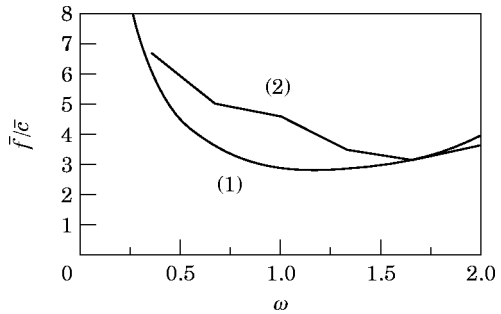


Figure 3. Regions of chaos from (1) theory and (2) numerical simulation.

or in vector form, $\dot{q} = f(q) + \epsilon g(q, t; \mu)$, where $0 < \epsilon \ll 1$, $\omega \in R$, $q = (x_1, x_2, z)$, $f = (f_1, f_2, 0)$ and $g = (g_1, g_2, \omega)$ are sufficiently smooth ($C^r$, $r \geqslant 2$ is adequate) and bounded on bounded sets, $f$ is periodic in $Z$ with periodic $T_1$, $g$ is periodic in $Z$ and $t$ with periods $T_1$ and $T_2$, respectively, and $\mu \in R^k$ is a parameter vector. The expression for the Melnikov function $(t_0, Z)$ is

$$M(t_0, Z) = \int_{-\infty}^{\infty} \left\{ f_1(q_0^z(t)) g_2(q_0^z(t), t + t_0) - f_2(q_0^z(t)) g_1(q_0^z(t), t + t_0) \right.$$

$$\left. + t\omega \left[ f_1(q_0^z(t)) \frac{\partial f_2}{\partial Z}(q_0^z(t)) \frac{\partial f_1}{\partial Z}(q_0^z(t)) \right] \right\} \mathrm{d}t \tag{48}$$

where $q_0^z(t)$ is the unperturbed homoclinic orbit. Suppose that there exists a point $(\bar{t}_0, \bar{Z})$ at which the following two conditions hold: (1) $M(\bar{t}_0, \bar{Z}) = 0$; (2) $DM(\bar{t}_0, \bar{Z})$ has maximal rank (i.e., $(\partial M/\partial t_0) M(\bar{t}_0, \bar{Z}) \neq 0$ and/or $(\partial M/\partial Z)(\bar{t}_0, \bar{Z}) \neq 0$). Then there exists $\epsilon_0$ such that, for $0 < \epsilon < \epsilon_0$, the stable manifolds transversely intersect unstable manifolds at point $(\bar{t}_0, \bar{Z}) + O(\epsilon)$.

The unperturbed system for equations (46) is given by

$$\dot{x} = x_2, \qquad \dot{x}_2 = (1 + \gamma \sin Z) \sin x_1, \qquad \dot{Z} = 0 \tag{49}$$

and is Hamiltonian, with the Hamiltonian function given by

$$H(x_1, x_2; Z) = x_2^2/2 - (1 + \gamma \sin Z)\cos(x_1 + \pi). \tag{50}$$

The unperturbed system has centers at $(x_1, x_2) = (\pm\pi, 0)$ and a saddle point at $(0, 0)$. The unperturbed homoclinic orbits are given by

$$\begin{aligned} q^0(t) &= (x_1(t), x_2(t)), \\ x_1(t) &= \pm 2 \sin^{-1}[\tanh(\sqrt{1 + \gamma \sin Z}\, t)] - \pi, \\ x_2(t) &= \pm 2\sqrt{1 + \gamma \sin Z}\, \operatorname{sech}(\sqrt{1 + \gamma \sin Z}\, t). \end{aligned} \tag{51}$$

Using the form in (48), one has

$$M(t_0, Z) = \int_{-\infty}^{\infty} [-\bar{c}(x_2(t))^2 - (\omega t x_2)\gamma \cos Z \sin(x_1(t))]\, \mathrm{d}t$$

$$= -4(1 + \gamma \sin Z)\bar{c} \int_{-\infty}^{\infty} \operatorname{sech}^2(\sqrt{1 + \gamma \sin Z}\, t)\, \mathrm{d}t$$

$$-4\sqrt{1 + \gamma \sin Z} \int_{-\infty}^{\infty} \tanh(\sqrt{1 + \gamma \sin Z}\, t) \operatorname{sech}^2(\sqrt{1 + \gamma \sin Z}\, t)\, \mathrm{d}t$$

$$-8\bar{c}\sqrt{1 + \gamma \sin Z} + \frac{4\gamma\omega \cos Z}{\sqrt{1 + \gamma \sin \mathrm{t}Z}}. \tag{52}$$

Using the Melnikov theorem, and after some algebra, one obtains an equation the graph of which in $(\bar{c}, \gamma, \omega)$ space is a surface above which transverse homoclinic orbits occur. This equation is (see Appendix B)

$$\gamma = \frac{2\bar{c}/\omega}{\sqrt{1 + (2\bar{c}/\omega)^2}}. \tag{53}$$

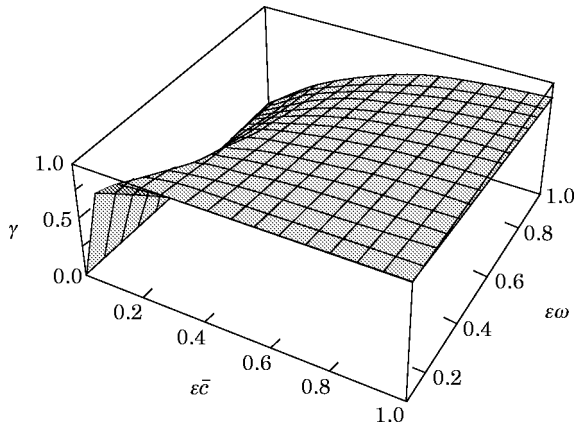


Figure 4. The graph in $(\gamma, \epsilon\bar{c}, \epsilon\omega)$ space is a surface above which transverse homoclinic orbits occur.

The surface shown in Figure 4 is such that homoclinic tangencies occur on it and transverse homoclinic orbits occur above it.

## 5. NUMERICAL SIMULATIONS AND DISCUSSION

In the present study, the non-linear equation of motion (7) were integrated numerically in order to obtain the various forms of dynamic behavior of the gyroscope. A fourth order Runge–Kutta integration algorithm has been used. Bifurcation diagrams, phase diagrams, Poincaré map, power spectrum analysis and Liapunov exponents are all modern techniques used in the analysis of non-linear deterministic systems. In this section, the above techniques are adopted to examine various forms of dynamical behavior of the present system. The dynamics may be viewed globally over a range of parameter values, thereby allowing simultaneous comparsion of periodic and chaotic forms of behavior. The bifurcation diagram provides a summary of the essential dynamics and is therefore a useful method for acquiring this overview.

For this system, bifurcation can easily be detected by examining a graph of $\dot{\theta}$ versus the normalized amplitude of the external harmonic excitation for specific values of the parameters $\alpha$, $\beta$, $c$ and $\omega$ (the frequency of the external harmonic excitation). The bifurcation will be obtained by the fourth order Runge–Kutta numerical integration algorithm with 20 initial conditions. At each value of the normalized amplitude $\bar{f} = Mg\bar{l}/I_1$ of the external harmonic excitation, the first 300 points of the Poncaré map are discarded in order to exclude the transient state of motion. After that, the system is seen to be in the steady state and the velocities for the next 200 points are plotted on the bifurcation diagram. Only the stable limit set is plotted. The bifurcation diagrams for two different specific value sets ((A) $\alpha^2 = 0$, $\beta = 1$, $c = 0{\cdot}5$, $\omega = 2/3$; (B) $\alpha^2 = 100$, $\beta = 1$, $c = 0{\cdot}5$, $\omega = 2$) are presented in Figures 5(a) and (b). Suppose that system (A) is lightly disturbed (say, $f = 2{\cdot}1$). The phase trajectory converges to the fixed point $(\pi, 0)$; the corresponding Poincaré section shows a fixed point, as shown in Figures 6(a) and (b), respectively. If the normalized amplitude is increased to approximately 2·56, explosive bifurcation occurs (Fig. 5(a)), which indicates that there is a discontinuous increase in the size and form of a strange attractor, the new enlarged attractor, after bifurcation, which includes within itself the phase space regime of the old attractor [13]. The phase trajectory and Poincaré map for

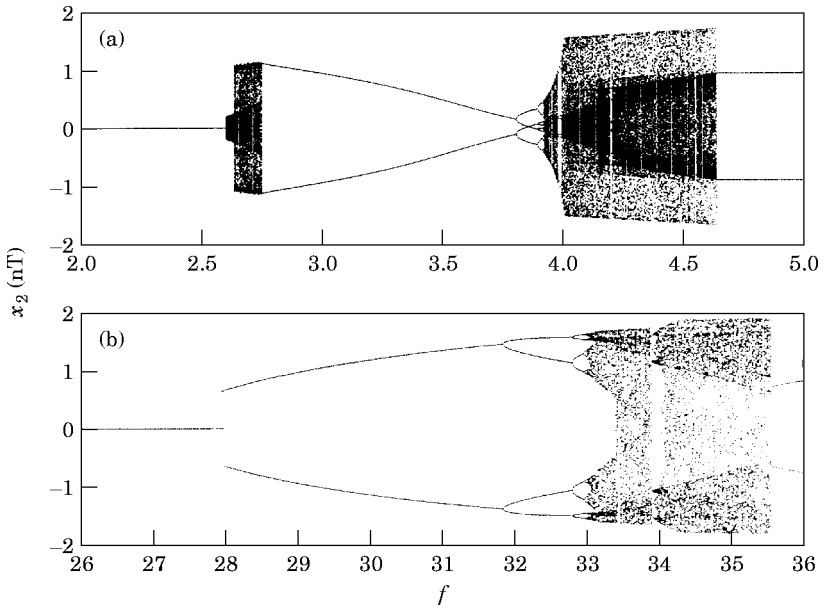


Figure 5. Gyroscope bifurcation diagrams for two different specific values set [(A) $\alpha^2 = 0$, $\beta = 1$, $c = 0{\cdot}5$, $\omega = 2/3$; (B) $\alpha^2 = 100$, $\beta = 1$, $c = 0{\cdot}5$, $\omega = 2$]; steady state angular velocity $x_2$ (nT) versus the normalized amplitude $f$ of external excitation. (a) set (A); (b) set (B).

$f = 2{\cdot}56$ are shown in Figures 6(c) and (d). When $f$ is increased further, explosive phenomena disappear and regular motion returns. Further increases in $f$ produce the period doubling phenomenon. If $f$ is increased further, the diagram becomes very complex.

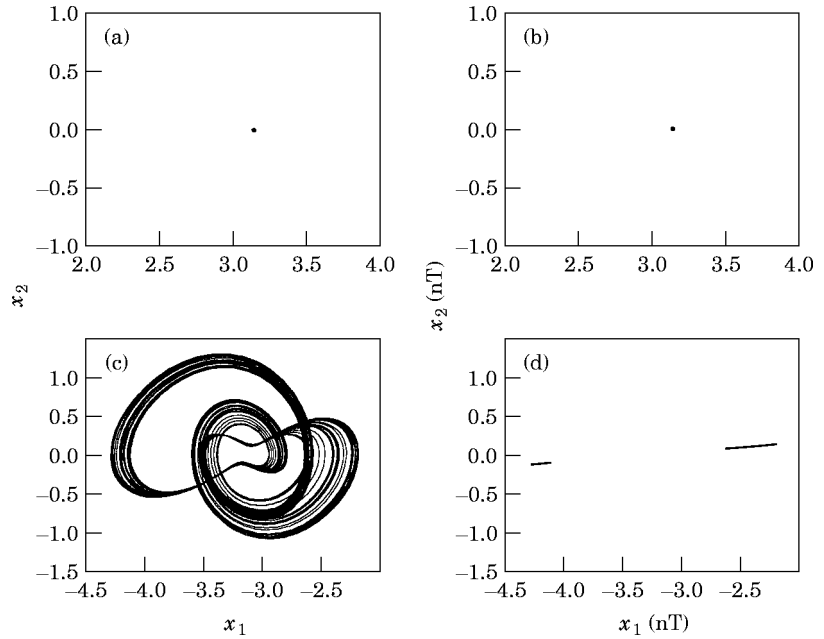


Figure 6. (a) The phase trajectory for $f = 2{\cdot}1$ in case (A); (b) the Poincaré map for $f = 2{\cdot}1$ in case (A); (c) the phase trajectory for $f = 2{\cdot}56$ in case (A); (d) the Poincaré map for $f = 2{\cdot}56$ in case (A).

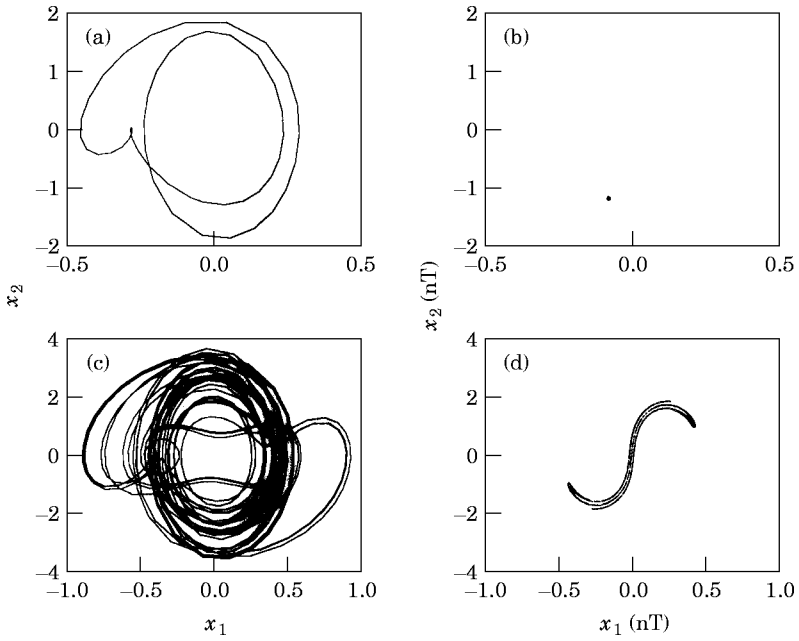


Figure 7. (a) The phase trajectory for $f = 33{\cdot}0$ in case (B); (b) the Poincaré map for $f = 33{\cdot}0$ in case (B); (c) the phase trajectory for $f = 34{\cdot}5$ in case (B); (d) the Poincaré map for $f = 34{\cdot}5$ in case (B).

In case (B), the period doubling bifurcation phenomenon is very easy to see. In Figures 7(a) and (b) are shown the phase trajectory and Poincaré map for $f = 30{\cdot}0$, and in Figures 7(c) and (d) are shown the phase trajectory and Poincaré map for $f = 34{\cdot}5$. However, when the bifurcation diagram loses continuity, this may lead to either quasi-periodic motion or chaotic motion, and further tests are required to classify the dynamics.

A chaotic signal has a power spectrum which shows a random broadband character. In Figure 8(a) and (b) are shown the time history and power spectrum for $\alpha^2 = 100$, $\beta = 1$, $c = 0{\cdot}5$, $\omega = 2$ and $f = 34{\cdot}5$. The power spectrum of chaotic oscillation is continuous broadband, as expected.

## 6. LIAPUNOV EXPONENTS

A variety of observations over time of Poincaré maps, phase diagrams and bifurcation diagrams have shown that the present system has a periodic and a fixed point character. However, the above techniques sometimes cannot clearly reveal whether the system is in quasi-periodic or chaotic motion; therefore, quantifying chaos has become an important problem. Liapunov exponents can provide a qualitative and quantitative characteristic of dynamic behavior. An algorithm for calculating the Liapunov exponents has been developed [14]. Liapunov exponents are very convenient for explaining the chaotic behavior of the system under consideration. Spectral analysis of Liapunov exponents has proven to be the most useful dynamical diagnostic tool for examining chaotic motions. The Liapunov exponents $\lambda_i$, which are simple constants, are the average exponential rates of divergence or convergence of nearby orbits corresponding to nearly identical states. In other words, if $\lambda$ is negative, slightly separated trajectories converge and evolution is not chaotic. If $\lambda$ is positive, nearby trajectories diverge; and evolution is sensitive to initial conditions and therefore chaotic; i.e., the system will soon behave quite differently and

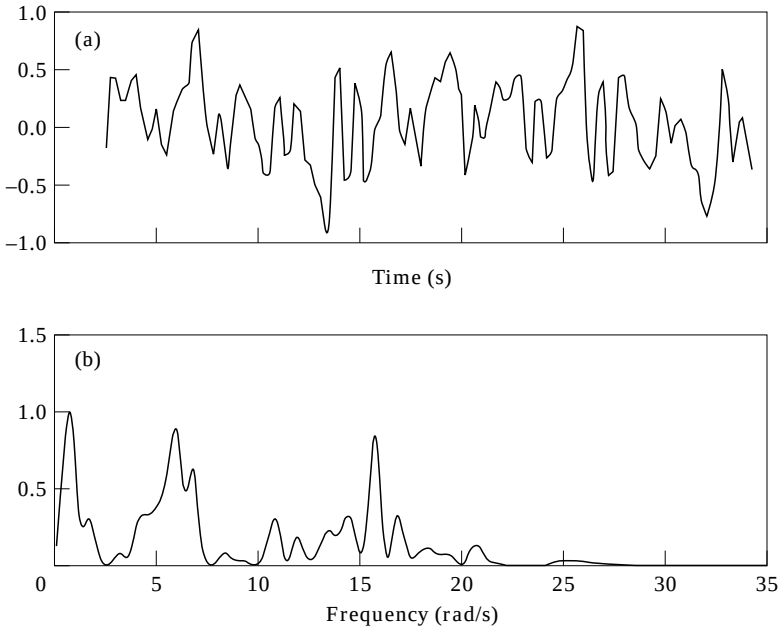


Figure 8. The trajectory and average power spectra for $\alpha^2 = 100$, $\beta = 1$, $c = 0{\cdot}5$, $\omega = 2$, $f = 34{\cdot}5$.

predictive ability will be rapidly lost. For a dissipative system, the sum of the exponents must be negative and equal to the damping coefficient of the system. If $x_3 = \omega t$ is introduced, then the non-autonomous equation (8) of motion can be transformed as autonomous ones:

$$\dot{x}_1 = x_2, \qquad \dot{x}_2 = -\alpha^2 \frac{(1 - \cos x_1)^2}{\sin^3 x_1} - cx_2 + \beta \sin x_1 + f \sin x_3 \sin x_1, \qquad \dot{x}_3 = \omega. \quad (54)$$

For example, in the phase space $(x_1, x_2, x_3)$ the Liapunov exponents for the system are found to be $\lambda_1 = 0{\cdot}1207$, $\lambda_2 = -0{\cdot}6207$ and $\lambda_3 = 0$ (when $f = 4{\cdot}5$, in case (A)). In this system the sum of all three Liapunov exponents, $\lambda_1 + \lambda_2 + \lambda_3 = -0{\cdot}5$, is equivalent to the negative damping coefficient of the system, independently of position and time [15]. In Tables 1 and 2 are shown the Liapunov exponents of the system using various values of $f$ (normalized amplitude) for two different sets of specific system values (A), $\alpha^2 = 0$, $\beta = 1$, $c = 0{\cdot}5$, $\omega = 2/3$; and (B), $\alpha^2 = 100$, $\beta = 1$, $c = 0{\cdot}5$, $\omega = 2$). The Liapunov spectra for two

TABLE 1

*The Liapunov exponents for a gyroscope using various values of f in case (A)*

| $f$ | $\lambda_1$ | $\lambda_2$ | $\lambda_3$ | $-\Sigma\,\lambda$ |
|---|---|---|---|---|
| 2·0 | −0·1558 | −0·3442 | 0·0 | 0·5 |
| 2·5 | −0·0130 | −0·4870 | 0·0 | 0·5 |
| 3·0 | −0·1074 | −0·3926 | 0·0 | 0·5 |
| 3·5 | −0·2484 | −0·2516 | 0·0 | 0·5 |
| 4·0 | 0·0350 | −0·5350 | 0·0 | 0·5 |
| 4·5 | 0·1207 | −0·6207 | 0·0 | 0·5 |
| 5·0 | −0·1309 | −0·3691 | 0·0 | 0·5 |

TABLE 2

*The Liapunov exponents for a gyroscope using various values of f in case (B)*

| $f$ | $\lambda_1$ | $\lambda_2$ | $\lambda_3$ | $-\Sigma\,\lambda$ |
|---|---|---|---|---|
| 33·0 | −0·0328 | −0·4672 | 0·0 | 0·5 |
| 33·5 | 0·1794 | −0·6794 | 0·0 | 0·5 |
| 34·0 | 0·0275 | −0·5275 | 0·0 | 0·5 |
| 34·5 | 0·2087 | −0·7087 | 0·0 | 0·5 |
| 35·0 | 0·2418 | −0·7418 | 0·0 | 0·5 |
| 35·5 | 0·2843 | −0·7843 | 0·0 | 0·5 |
| 36·0 | −0·2235 | −0·2765 | 0·0 | 0·5 |

different specific system parameter value sets are shown in Figures 9(a) and (b) to confirm the chaotic dynamics.

## 7. THE EFFECT OF THE GYROSCOPE'S SPIN VELOCITY

The extreme sensitivity to initial states in a system operating in chaotic mode can be very destructive for the system because of unpredictable behavior. As a result, it is essential to know when a non-linear system will enter a chaotic mode—so as to avoid it—and how to recover from it. In other works, how can chaotic systems be driven to any point in phase space and maintained at that point for long periods?

In Figure 10 are shown the Poincaré maps of a gyroscope with $\beta = 1$, $c = 0{\cdot}5$ and $\omega = 2$. Here one is interested in the effect of the gyroscope's spin velocity on the various dynamic behaviors of the system. Therefore, the parameter $f = 35{\cdot}5$ was fixed, and the parameter $\alpha = (I_3/I_1)\omega_z$ (where $\omega_z$ is the spinning velocity) varied. In Figure 10(a) is shown a Poincaré

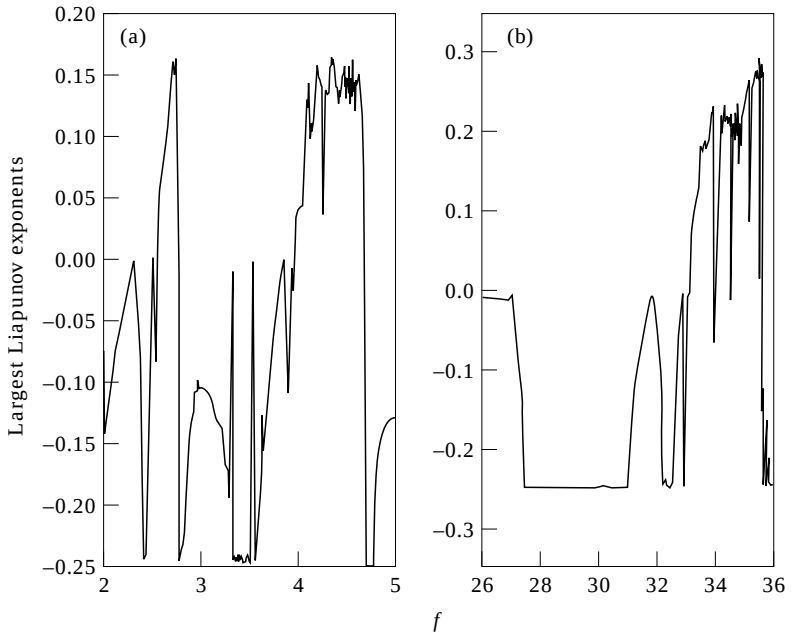


Figure 9. The largest Liapunov exponents as a function of $f$ for (a) set (A) and (b) set (B).

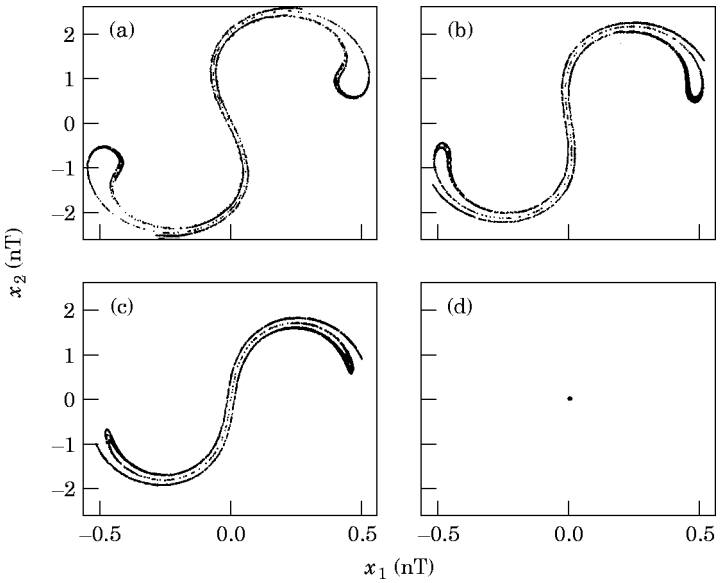


Figure 10. Poincaré maps (parameters $\beta = 1$, $c = 0{\cdot}5$, $\omega = 2$, and fixed the parameter $f = 35{\cdot}5$): (a) $\alpha^2 = 90$; (b) $\alpha^2 = 95$; (c) $\alpha^2 = 100$; (d) $\alpha^2 = 110$.

map with $\alpha^2 = 90$. Progressive increases in $\alpha^2$ resulted firstly, in the "strange attractor" regions being decreased, as shown in Figures 10(b) ($\alpha^2 = 95$) and (c) ($\alpha^2 = 100$). When $\alpha^2$ is increased further (say, $\alpha^2 = 110$), the chaotic motion disappears, and regularity returns, as shown in Figure 10(d). This shows that the spin velocity has a significant effect on the dynamic behavior of the present system, and points to a finding that has practical importance for gyroscope design.

## 8. CONCLUSIONS

The non-linear motion of a symmetric gyro mounted on a vibrating base has been investigated. It was shown that the system exhibited both regular and chaotic motions. The stability of the system has been studied according to the damped Mathieu equation theory. The complete equation of motion is a highly non-linear non-autonomous one. It is difficult to find a positive definite Liapunov function, since the Liapunov direct method was used. However, this difficulty was overcome in Section 3. The Liapunov direct method was also employed in a rigorous treatment of sufficient conditons for system stability. When the system was subjected to external disturbance, the Melnikov method was used to show the existence of chaotic motion. Finally, the bifurcation of the parameter dependent system was studied numerically. The time evolutions of the non-linear dynamical system response were described using the phase portraits via the Poincaré map technique. The occurrence and nature of chaotic attractors were verifed by evaluating Liapunov exponents and average power spectra. The effect of the gyroscope's spin speed was also studied. It was shown that spin velocity $\omega_z$ of the gyroscope has a significant effect on the dynamic behavior of the motion; e.g., chaotic motion tends to disappear increasingly as the spin velocity increases. This removed the chaos from this system, allowing it to stabilize and exhibit predictable behavior. This is obviously of significance for the design of future gyroscopes.

ACKNOWLEDGMENT

This research is supported by the National Science Council, Republic of China, under Grant Number NSC 85-2212-E-009-014.

REFERENCES

1. R. B. Leipnik and T. A. Newton 1981 *Physics Letters* **86A**, 63–67. Double strange attractors in rigid body motion with feedback control.
2. H. Poincaré 1899 *Les Methodes Nouvelles de La Mecanique* (three volumes). Paris: Gauthier-Villiars.
3. E. N. Lorenz 1963 *Journal of Atmospheric Science* **20**, 130–140 Deterministic nonperiodic flow.
4. F. C. Moon 1992 *Chaotic and Fractal Dynamics*. New York: John Wiley.
5. J. M. T. Thompson and H. B. Stewart 1987 *Nonlinear Dynamics and Chaos*. New York: John Wiley.
6. H. Gunderson, H. Rigas and F. S. Vanvleck 1974 *SIAM Journal of Applied Mathematics* **26**, 345–349. A technique for determining stability regions for the damped Mathieu equation.
7. M. Vidyasagar 1993 *Nonlinear Systems Analysis*. London: Prentice-Hall.
8. J. Guckenheimer and P. J. Holmes 1983 *Nonlinear Oscillations*, *Dynamical Systems*, *and Bifurcations of Vector Fields*. New York: Springer-Verlag.
9. F. R. Gantmacher *Lectures on Analytical Mechanics*. New York: Chelsea; second edition.
10. A. H. Nayfeh and B. Balachandran 1994 *Applied Nonlinear Dynamics*. New York: John Wiley.
11. L. Cveticanin 1995 *Transactions of the ASME*, *Journal of Applied Mechanics* **62**, 227–229. A note on the stability and instability of system with time variable parameters.
12. S. Wiggins 1988 *Global Bifurcations and Chaos*. New York: Springer-Verlag.
13. J. M. T. Thompson, H. B. Stewart and Y. Ueda 1994 *Physical Review E* **49**, 1019–1027. Safe, explosive, and dangerous bifurcations in dissipative dynamical systems.
14. Wolf, J. B. Swift, H. L. Swinney and J. A. Vastano 1985 *Physica* **D16**, 285–317. Determining Liapunov exponents from a time series.
15. L. Baker and J. P. Gollub 1990 *Chaotic Dynamics*, *an Introduction*. Cambridge University Press.

## APPENDIX A

In Section 4, the unperturbed form for equation (32) is

$$\dot{x}_1 = x_2, \qquad \dot{x}_2 = \sin x_1. \tag{A1}$$

The fixed points are (A) $x_1 = x_2 = 0$ and (B) $x_1 = \pm\pi$, $x_2 = 0$. In the neighborhood of $x_1 = x_2 = 0$, equation (A1) reduces to

$$\dot{x}_1 = x_2, \qquad \dot{x}_2 = x_1. \tag{A2}$$

The corresponding characteristic equation is

$$\lambda^2 - 1 = 0. \tag{A3}$$

which has the roots $\lambda_1, \lambda_2 = \pm 1$. Because the roots are real but opposite in sign, the fixed point is a saddle point.

In the neighborhood of $x_1 = \pm\pi$, $x_2 = 0$, equation (A1) becomes

$$\dot{x}_1 = x_2, \qquad \dot{x}_2 = -x_1. \tag{A4}$$

The characteristic equation is simply

$$\lambda^2 + 1 = 0. \tag{A5}$$

which has the roots $\lambda_1, \lambda_2 = \pm \mathrm{i}$. Because the roots are pure imaginary complex conjugates, one can conclude that the system has centers at $(x_1 = \pm\pi, x_2 = 0)$. A phase portrait is

structurally stable if its toplogy cannot be changed by an arbitrarily small perturbation to the vector field. For instance, the phase portrait of a saddle point is structurally stable but that of a center is not: an arbitrary small amount of damping converts the center to a spiral.

## APPENDIX B

From Section 4, for case (B) $F(t) = \gamma \sin \epsilon\omega t$, while Melnikov function is

$$M = -8\bar{c}\sqrt{1 + \gamma \sin Z} + \frac{4\gamma\omega \cos Z}{\sqrt{1 + \gamma \sin Z}}. \tag{B1}$$

According to the modified Melnikov theorem, when the stable manifolds transversely intersect the unstable manifolds, the conditions $M = 0$ must hold. Therefore, the following equation,

$$-8\bar{c}\sqrt{1 + \gamma \sin Z} + \frac{4\gamma\omega \cos Z}{\sqrt{1 + \gamma \sin Z}} = 0, \tag{B2}$$

is satisfied. One finds that

$$2\bar{c}/\gamma = \omega \cos Z - 2\bar{c} \sin Z = \sqrt{\omega^2 + 4\bar{c}^2} \cos (Z + Z_1), \tag{B3}$$

where $Z_1 = \tan^{-1} (\omega/2\bar{c})$. At $Z = -Z_1$, one has

$$2\bar{c}/\gamma = \sqrt{\omega^2 + 4\bar{c}^2}, \tag{B4}$$

i.e.,

$$\gamma = \frac{2\bar{c}/\omega}{\sqrt{1 + (2\bar{c}/\omega)^2}}. \tag{B5}$$